A Bonner Sphere Spectrometer based on a large ^{6}LiI(Eu) scintillator: Calibration in reference monoenergetic fields

R. Bedogni [a,*], A. Pola [b,c], M. Costa [d,e], V. Monti [d,e], D.J. Thomas [f]

[a] INFN – LNF, via E. Fermi n. 40, 00044 Frascati (Roma), Italy
[b] Politecnico di Milano, Dipartimento di Energia, via La Masa 34, 20156 Milano, Italy
[c] INFN – Milano, Via Celoria 16, 20133 Milano, Italy
[d] INFN Sezione di Torino, via Pietro Giuria 1, 10125 Torino, Italy
[e] Università degli Studi di Torino, Via P. Giuria 1, 10125 Torino, Italy
[f] National Physical Laboratory, Hampton Road, TW11 0LW Teddington, Middlesex, UK

ARTICLE INFO

Keywords:
Neutron spectrometry
Neutron dosimetry
Monoenergetic neutrons

ABSTRACT

A Bonner Sphere spectrometer employing a large, 11 mm diameter × 3 mm thickness, ^{6}LiI(Eu) scintillator (LL-BSS), was assembled. The purpose was to produce a BSS similar in sensitivity to those based on ^{3}He sensors, but using alternative sensors. With respect to the traditional BSS based on the 4 mm (diameter) × 4 mm (height) ^{6}LiI(Eu), this new BSS is a factor of 3 more sensitive. LL-BSS response matrix, determined with MCNPX, was experimentally evaluated with monoenergetic reference neutron fields of 144 keV, 565 keV and 1.2 MeV available at NPL (Teddington, UK). The results of the experiment confirmed the correctness of the response matrix within an overall uncertainty lower than ±2%.

1. Introduction

Bonner Spheres (BS) were invented at Rice University by Bramblett et al. [1] in 1960. Since then, this spectrometer is still used more than any other in neutron dosimetry [2]. Very large energy range and isotropic response are the main advantages of this spectrometer. Other advantages are the possibility to choose in a variety of active and passive thermal sensors, to match the characteristics of a specific workplace, and a generally good photon rejection Main disadvantages are the poor energy resolution, the sequential exposure of the spheres, leading to time consuming irradiation sessions, and the need of complex "unfolding" procedures to reconstruct the spectrum from the experimental data.

The accuracy of BS largely depends on the exact knowledge of the sphere response functions. The response function of a given sphere is defined as the counts in the central detector, per unit incident neutron fluence, when the sphere is uniformly irradiated. This is function of the neutron energy. The response functions of all spheres form the response matrix. The response functions are usually calculated by Monte Carlo transport codes. Their accuracy can be experimentally evaluated, in the energy domain below 20 MeV, in reference monoenergetic neutron fields as those described in ISO [3] and available in few metrology institutes worldwide. To achieve accurate response functions, the following aspects need to be carefully controlled:

– The HDPE density [4],
– The materials and dimensions characterizing the sphere-detector assembly. Air gaps between detector and sphere also need to be accurately known.

For a well-simulated response matrix, typical differences between simulation and experiment in reference monoenergetic neutron fields are lower than 10% [5,6].

Since BS are frequently used to support radiation protection programs, a high-sensitivity central detector is desirable. In addition, this detector should be as photon insensitive as possible. The size of the detector should be very small, in order to allow small spheres (like 50–60 mm in diameter) to be used. Pressurized ^{3}He proportional counters have been frequently used in the past, but the supply restrictions and high cost of this isotope are orienting the scientific community toward cheaper alternatives, with acceptable sensitivity. Table 1 compares the sensitivity of different central detectors. This is represented by the response of the 200 mm diameter sphere (or 8 in.) at 1 MeV.

The 4 mm × 4 mm ^{6}LiI(Eu) is significantly less sensitive than ^{3}He-based detectors. Increasing its size would increase the sensitivity, but this was traditionally considered to negatively impact the photon sensitivity [2]. This paper shows that a "large" ^{6}LiI(Eu), 11 mm diameter × 3 mm height, with adequate electronic readout, can be used in most

* Corresponding author.
E-mail address: roberto.bedogni@lnf.infn.it (R. Bedogni).

Table 1
Sensitivity of different BS central detectors, represented by the response of the 200 mm diameter sphere (or 8 in.) at 1 MeV.

Central detector model	Sensitive volume and shape	R (1 MeV, 200 mm) cm^2	References
05NH1	8 kPa, ^{3}He Cylindrical, 10 mm × 9 mm	0.4	[7]
SP9	200 kPa, ^{3}He Spherical, 32 mm diameter	2.5	[8,9]
^{6}LiI(Eu)	Scintillator Cylindrical, 4 mm × 4 mm	0.2	[6,10]
^{6}LiI(Eu)	Scintillator Cylindrical, 11 mm × 3 mm	0.6	This work

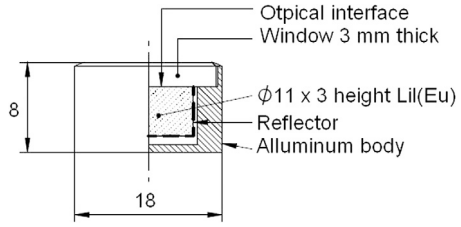

Fig. 1. Structure of the large ^{6}LiI(Eu) scintillator, 11 mm diameter × 3 mm height. All dimensions in mm. Courtesy of Scionix Holland BV.

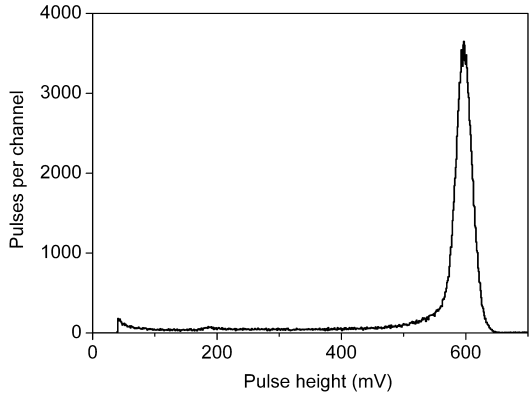

Fig. 2. Pulse height spectrum of the large ^{6}LiI(Eu) scintillator exposed to thermal neutrons.

operative scenarios. The BS based on this detector is here called LL-BSS (Large LiI(Eu) Bonner Sphere Spectrometer). Although its sensitivity is lower than that of the SP9-based BSS, it responds 50% more than the 05NH1 one, and is still very small compared with the size of the smaller spheres.

LL-BSS response matrix was derived with MCNPX [11] and experimentally validated with reference monoenergetic neutron fields at NPL.

2. The central detector

The LL-BSS central detector used in this work is produced by Scionix Holland BV. Its internal structure is shown in Fig. 1.

The optical window (glass) was coupled with a PM tube (10 mm diameter active window) through optical grease. The PM operates at positive 1100 V. The anode of the PM tube is directly connected to the analog input on a commercial digitizer (NI USB 6366X, BNC connectivity). In house LabView-based software was developed to process the signal from the detector. The anodic signal generated by thermal neutron events exhibits a steep rising front (<1 μs, corresponding to the time sample of the digitizer) followed by a slower decay. The software digitally processes the waveform from the PM anode and measures the height of the rising fronts. The Pulse height distribution (Fig. 2) is derived on this basis.

The system was found to be immune to pile up and saturation effects for counting rates up to at least 10^5 s^{-1}.

The main peak in the spectrum (Fig. 2) is due to the complete collection of both α (2.05 MeV, range in LiI 8 μm) and Triton (2.73 MeV, range in LiI 48 μm) products from the neutron capture reaction in ^{6}Li. The straggling component comes from the partial escape of the reaction products. As these partial escapes denote a genuine neutron capture event, an asymmetric Region of Interest (ROI) for counting purposes was extended from (centroid—5 FWHM) to (centroid +3 FWHM). The large photon-neutron separation allowed such a large ROI.

The secondary electrons from photon interactions are found in the falling tail located below 100 mV. A very large separation exists from photon and thermal neutron events, allowing for a high neutron-to-photon discrimination capability. Tests with ^{137}Cs sources showed that photon kerma rates up to at least 10 mGy h^{-1}do not influence the region of the spectrum where the neutron peak grows.

Explanations for this large neutron-gamma separation, with respect to the traditional 4 mm (diameter) × 4 mm (height) cylindrical counter, could be:

- With respect to the traditional analog chain (shaper amplifier, Multichannel Analyser), the one used in this work directly digitizes the anodic signal, thus reducing the sources of noise and signal broadening;
- With respect to the old counter, the new one improves the light collection efficiency because the ratio between the area in contact with the optical window and the detector volume is higher.

3. The response matrix

Bonner Spheres were manufactured using HDPE and their nominal diameters were (in mm) 60, 70, 80, 90, 100, 110, 125, 150, 170, 200, 250 and 300. Their average diameters and the dimensions of all mechanical features (such as the cavity for the detector) were accurately determined. The actual HDPE density was measured for every sphere with accuracy better than 1%.

The LL-BSS response matrix (Fig. 3) was determined with MCNPX by simulating an exposure with a uniform parallel neutron beam having the same diameter as the studied sphere, and impinging the sphere along the detector cylindrical axis. The ENDF/B-VII cross section library [12] below 20 MeV, and the room temperature S(α,β) cross sections for thermal treatment in polyethylene, were used. The Bertini intra nuclear cascade model and the Dresdner evaporation model were used above 20 MeV [13].

The simulated response (unit: cm^2) is here defined as, the number of (n,α) capture events in the central detector, per unit incident neutron fluence, as a function of the sphere size and of the monoenergetic neutron energy. Pedix "i", with $i = 1, \ldots, 12$, denotes the sphere.

Table 2
The main characteristics of the used beams.

Nominal monoenergetic energy (keV)	Full width of energy distribution (keV)	Reaction used	Measurement angle	Standard uncertainty on reference fluence at reference point	Target scatter fraction (% of the total fluence)
143.3 ± 4.6	14.4	^{7}Li(p, n)	0°	±2.3%	1.1%
565.6 ± 3.4	9.6	^{7}Li(p, n)	0°	±2.5%	0.6%
1201 ± 11	100	T(p, n)	0°	±2.9%	3.6%

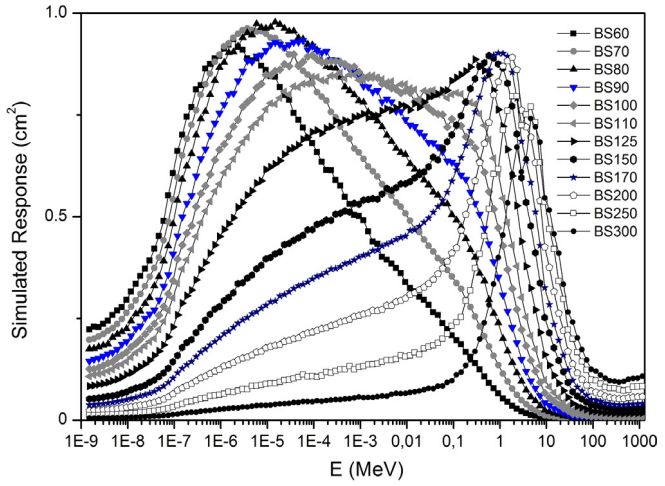

Fig. 3. Simulated response matrix of the LL-BSS. The experimental response $C_i(E)$ is given by $FM_i(E)$, where the F constant (the calibration factor) should not depend on the neutron energy and sphere size.

As expected, the shape of the LL-BSS response matrix is very similar to that of other BSSs described in literature.

As not all neutron captures in the crystal yield a measured pulse, the experimental response of the LL-BSS unit fluence, $C_i(E)$, will be lower than the corresponding simulated quantity $M_i(E)$. This can be attributed to multiple factors, such as the crystal-to-PM optical coupling, the difference between real and nominal size of the crystal, the exact crystal composition.

The ratio between observed and expected counts is hereafter called *spectrometer calibration factor*, F, and its value is lower than 1. Its experimental determination is one of the objectives of this work. If the simulation model is correct in terms of geometry, dimensions and materials, F will not depend from the sphere size and from the neutron energy.

For every monoenergetic energy used in this experiment, and for every sphere, an experimental estimation of the calibration factor $F_{i,E}$ (where i denotes the sphere and E the mono-chromatic energy) was performed. Its degree of constancy, when the sphere size and the neutron energy vary, is here regarded as the "overall accuracy" of the simulated response matrix in the studied energy range.

4. Irradiation conditions

The irradiation tests took place in the low-scatter irradiation room of NPL, using the 3.5 MV Van de Graaff accelerator operated by the Neutron Metrology Group. The exploited reactions were ^{7}Li(p, n) to generate 144 keV and 565 keV beams, and $T(p, n)$ for the 1.2 MeV beam. All measurements were done at 0° angle with respect to the direction of the accelerated beam. The distance from target to the sphere centre was 2 m. Eleven spheres (from 60 to 250 mm in diameter) were used in the experiment. The shadow-cone technique was used to subtract the air- and room-scatter contribution from the spectrometer readings.

The reference value of monoenergetic neutron fluence delivered to the reference point (sphere centre) was known through measurements with the Standard NPL long counter plus a suite of permanent monitor instruments.

The main characteristics of the used beams are summarized in Table 2.

The target scatter fraction, based on Monte Carlo simulations, can be assumed as affected by uncertainty up to ±40% [14]. These are neutrons with lower energy than the monoenergetic one. Since the long counter used to determine the reference fluence has flat energy dependence of the fluence response, the result is a slight overestimation of the monoenergetic fluence. This was taken into account in data analysis.

5. Results of the irradiation tests

For every monoenergetic energy (E) and every sphere (i), an estimation of the LL-BSS calibration factor $F_{i,E}$, was derived as follows.

If the beam was a pure monoenergetic one, $F_{i,E}$ could be simply derived by the formula (1)

$$F_{i,E} = \frac{\frac{C_{i,E,tot}}{\Phi_{i,E,tot}} - \frac{C_{i,E,cone}}{\Phi_{i,E,cone}}}{M_{i,E}} \quad (1)$$

where:

- $C_{i,E,tot}$ counts in the ith sphere in the total field irradiation;
- $\Phi_{i,E,tot}$ monoenergetic neutron fluence delivered at the reference point (sphere centre) during the total field irradiation (unit: cm^{-2});
- $C_{i,E,cone}$ the counts in the ith sphere in the irradiation with shadow cone;
- $\Phi_{i,E,cone}$ monoenergetic reference neutron fluence that would be delivered at the reference point during the irradiation with shadow cone, in absence of shadow-cone (unit: cm^{-2});
- $M_{i,E}$ simulated sphere response function at the energy E.

To be more precise, it should be considered that the target-scattered component is affecting both the value of fluence and the sphere counts, but not in the same way. Therefore, the fraction in Eq. (1) needs to be multiplied by a correction factor, f_s, elaborated on the basis of the expected monoenergetic and target scattered spectra, provided by NPL. f_s is defined as follows:

$$f_s = \frac{1 - TS\frac{R_{scatter}}{R_{scatter+mono}}}{1 - TS} \quad (2)$$

where:

- TS Target-scatter fraction (Table 2) in terms of fraction of total the fluence;
- $R_{scatter}$ Sphere response function folded with the scattered spectrum normalized to unit fluence;
- $R_{scatter+mono}$ Sphere response function folded with the total spectrum coming from the target, i.e. monoenergetic + target scattered, normalized to unit fluence.

f_s usually constitutes a small correction: its value is ranges from 0.991 ± 0.014 (BS60) to 1.004 ± 0.007 (BS250) for 144 keV, from 0.995 ± 0.008 (BS60) to 1.002 ± 0.004 (BS250) for 565 keV, and from 0.933 ± 0.071 to 1.018 ± 0.019 for 1.2 MeV.

The $F_{i,E}$ values experimentally obtained are reported in Table 3 for every monoenergetic energy

Table 3
$F_{i,E}$ values measured for every sphere and energy, and best estimation per energy.

	144 keV	565 keV	1.2 MeV
BS60	0.695 ± 4.6%	0.684 ± 4.2%	Not done
BS70	0.715 ± 4.1%	0.698 ± 3.6%	0.742 ± 8.3%
BS80	0.703 ± 3.9%	0.710 ± 3.4%	0.734 ± 7.2%
BS90	0.719 ± 3.8%	0.705 ± 3.2%	0.737 ± 6.4%
BS100	0.708 ± 3.7%	0.707 ± 3.1%	0.727 ± 5.8%
BS110	0.720 ± 3.6%	0.699 ± 3.1%	0.731 ± 5.5%
BS125	0.685 ± 3.5%	0.682 ± 3.0%	0.709 ± 5.0%
BS150	0.715 ± 3.4%	0.701 ± 2.9%	0.714 ± 4.5%
BS170	0.710 ± 3.4%	0.700 ± 2.9%	0.722 ± 4.3%
BS200	0.702 ± 3.4%	0.711 ± 2.8%	0.722 ± 4.0%
BS250	0.657 ± 3.3%	0.651 ± 2.8%	0.726 ± 3.8%
F_E	0.701 ± 2.5%	0.694 ± 2.7%	0.724 ± 3.3%
$F = 0.703 \pm 1.6\%$			

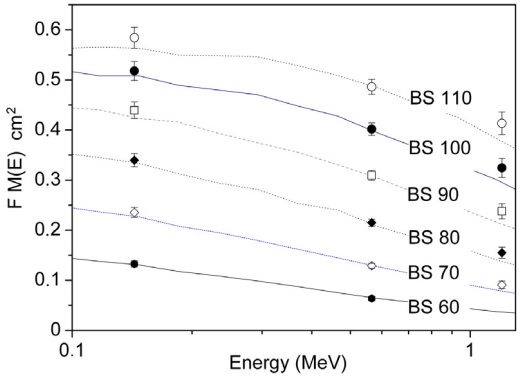

Fig. 4. Comparing the experimental (points) and simulated (lines) response function for the spheres from BS 60 to BS 100. Error bars refer to one sigma.

The best estimation of the calibration factor was derived for every energy, using the inverse square of uncertainty as weighting factors. This corresponds to F_E in Table 3 Uncertainties of F_E values are mainly due to fluence uncertainties (from Table 2).

The global calibration factor, F (last line of Table 3), was then obtained by a weighted average of the F_E values Its numerical value is $F = 0.703 \pm 0.011$ (±1.6%). The ±1.6% figure can be regarded as an estimation of the "overall uncertainty" of the simulated response matrix for the investigated energy range.

Figs. 4 and 5 compare, for the different spheres and energy, the experimental response function $(\frac{c_{i,E,tot}}{\Phi_{i,E,tot}} - \frac{c_{i,E,cone}}{\Phi_{i,E,cone}})\ f_s$ and the simulated one (corrected with the calibration factor), $F\ M_{i,E}$. The comparison is satisfactory.

6. Conclusions

A Bonner Sphere spectrometer employing a "large" (11 mm diameter × 3 mm thickness) ^{6}LiI(Eu) scintillator (LL-BSS), was developed and calibrated in monoenergetic reference fields of 144 keV, 565 keV and 1.2 MeV at NPL. The central detector, directly coupled to a digitizer, exhibits a very clean pulse height distribution with a very large separation from neutron to photon events. With respect to the traditional BSS based on the 4 mm (diameter) × 4 mm (height) ^{6}LiI(Eu), this new BSS is a factor of 3 more sensitive. An accurate MCNP model of the LL-BSS was used to generate a 120 equilethargic groups theoretical response matrix (from 1E-9 to 1E+3 MeV). The measurements showed that the overall uncertainty of this matrix in the studied energy range is lower than ±2%. Further work is planned to introduce metal-loaded spheres for high-energy neutrons, and to extend the range of validation to 10–20 MeV and higher energies.

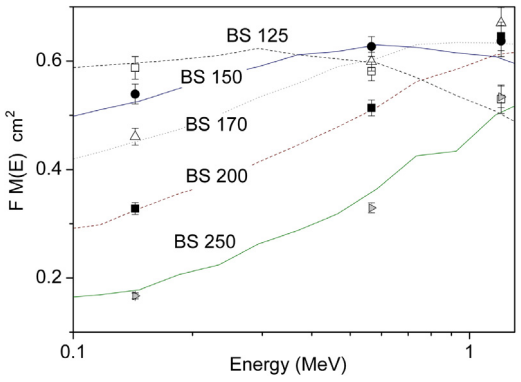

Fig. 5. Comparing the experimental (points) and simulated (lines) response function for the spheres from BS 125 to BS 250. Error bars refer to one sigma.

Acknowledgements

This work has been supported by projects INFN-E and E_LIBANS from INFN (Commissione Scientifica Nazionale 5). The staff of the NPL Neutron metrology Group is greatly acknowledged.

References

[1] R.L. Bramblett, R.I. Ewing, T.W. Bonner, Nucl. Instrum. Methods Phys. Res. 9 (1960) 1.
[2] A.V. Alevra, D.J. Thomas, Radiat. Prot. Dosim. 107 (2003) 33.
[3] ISO 8529-1, International Organization for Standardization. Reference neutron radiations e Part 1: characteristics and methods of production. International Standard ISO 8529-1, 2001.
[4] D.J. Thomas, A.V. Alevra, Nucl. Instrum. Methods Phys. Res. A 476 (2002) 12.
[5] R.M. Howell, E.A. Burgett, B. Wiegel, N.E. Hertel, Radiat. Meas. 45 (2010) 1233.
[6] V. Mares, H. Schraube, Nucl. Instrum. Methods Phys. Res. A 337 (1994) 461.
[7] V. Lacoste, V. Gressier, J.-L. Pochat, F. Fernandez, M. Bakali, T. Bouassoule, Radiat. Prot. Dosim. 110 (2004) 529.
[8] B. Wiegel, A.V. Alevra, Nucl. Instrum. Methods Phys. Res. A 476 (2002).
[9] S. Barros, V. Mares, R. Bedogni, M. Reginatto, A. Esposito, I.F. Gonçalves, P. Vaz, W. Rühm, Radiat. Prot. Dosim. 161 (2014) 46.
[10] A. Pola, D. Bortot, M.V. Introini, R. Bedogni, A. Gentile, A. Esposito, J.M. Gómez-Ros, E. Passoth, A. Prokofiev, Radiat. Prot. Dosim. 161 (2014) 229.
[11] D.B. Pelowitz, MCNPX User's Manual Version 2.7., Report LA-CP-11-00438, 2011.
[12] M.B. Chadwick, P. Oblozinsky, M. Herman, Nucl. Data Sheets 107 (2006) 2931.
[13] C. Pioch, V. Mares, W. Rühm, Radiat. Meas. 45 (2010) 1263.
[14] National Physica Laboratory, NPL. Certificate of calibration N1438. 1st December 2016.